

See discussions, stats, and author profiles for this publication at: <https://www.researchgate.net/publication/304743394>

# A Numerical Study of Low Reynolds Number Incompressible Flow at Entrance and Disturbed Regions Of Concentric Circular Pipes

Research · July 2016

DOI: 10.13140/RG.2.1.2797.2082

CITATIONS

0

READS

39

1 author:



Ahmed Al-Saadi

University of Leeds

4 PUBLICATIONS 11 CITATIONS

SEE PROFILE

Some of the authors of this publication are also working on these related projects:



Simulation of Aerodynamic Behaviour of a Super Utility Vehicle in Turbulent Flow [View project](#)

## **A Numerical Study of Low Reynolds Number Incompressible Flow at Entrance and Disturbed Regions Of Concentric Circular Pipes**

Ahmed Ali Shaker  
College of Engineering  
Al-Qadissiya University  
Mechanical Engineering Department  
[ahmedalsaadi78@gmail.com](mailto:ahmedalsaadi78@gmail.com)

### **Abstract:**

*The developing laminar flow in the entrance and disturbed regions of concentric circular pipes has been studied numerically. Both main pipe and disturbed pipe are concentric and stationary. Uniform developing flow occurs in entrance region of main pipe and inside disturbed pipe at disturbed region. while non-uniform developing flow occurs in annular concentric disturbed pipe at disturbed region. For the two-dimensional problem, numerical solutions are obtained for a wide range of Reynolds number from 25 to 375. A computer program and AutoFEA software were used to calculate the velocity and pressure drop within the entire channel. The maximum velocity at the centerline of the pipe, hydrodynamic boundary layer developed faster for the lower Reynolds number. However, the flow field is similar for all studied cases. All the present work data are in good agreement with AutoFEA software.*

**Keywords:** entrance region, disturbed flow, incompressible, circular pipe

دراسة عددية لمائع لا انضغاطي بعدد رينولدز واطئ عند منطقة المدخل و منطقة الاعتراض بأنبوبين دائريين متحدي المركز

### **الخلاصة**

الجريان الطبائقي النامي في منطقة المدخل ومنطقة الاعتراض بأنبوبين دائريين متحدي المركز درساً بشكل عددي. الأنبوب الرئيسي والأنبوب الاعتراضي كلاهما متحداً المركز و ثابتان. يحدث التدفق النامي المنتظم في منطقة مدخل الأنبوب الدائري الرئيسي وفي منطقة الاعتراض داخل الأنبوب الاعتراضي متحد المركز. يحدث التدفق النامي غير المنتظم في المنطقة الحلقية من أنبوب الاعتراض الدائري متحد المركز في منطقة الاعتراض. الحلول العددية ثنائية الأبعاد تمت لمدى واسع من أرقام رينولدز تبدأ من 25 إلى 375. تم استخدام برنامج بيسك و برنامج AutoFEA لحساب السرعة و الهبوط بالضغط ضمن القناة. نلاحظ ان أقصى سرعة عند محور الأنبوب و الطبقة المتاخمة تنمو أسرع عند استخدام أعداد رينولدز صغيرة طالما ان حقل التدفق مماثل لكل الحالات المدروسة. كل بيانات البحث الحالية انسجمت بشكل جيد مع قيم AutoFEA software.

## Nomenclature

The following symbols are used generally throughout the text. Other are defined as when used.

Symbol	Definition	Unit
d	Diameter of main circular pipe.	m
$L_d$	Hydrodynamic Disturbed Length	m
$L_e$	Hydrodynamic Entry Length	m
m	Number of Grid Nodes in the Axial Direction	
n	Number of Grid Nodes in the Radial Direction	
p	Pressure	N/m <sup>2</sup>
P	Dimensionless Pressure	
$p_o$	Initial Pressure	N/m <sup>2</sup>
r	Radius of circular pipe	m
R	Dimensionless Radius of circular pipe	
Re	Reynolds Number	
u	Velocity in Axial Direction	m/s
$u_o$	Initial Velocity in Axial Direction	m/s
U	Dimensionless Velocity in Axial Direction	
$U_o$	Initial Dimensionless Velocity in Axial Direction	
v	Velocity in Radial Direction	m/s
V	Dimensionless Velocity in Radial Direction	
z	Axial Direction of the circular pipe.	m
Z	Dimensionless Axial Direction of the circular pipe.	
$\Delta r$	The Distance Between Two Nodal Points in the Radial Direction	m
$\Delta R$	The Dimensionless Distance Between Two Nodal Points in the Radial Direction	
$\Delta z$	The Distance Between Two Nodal Points in the Axial Direction	m
$\Delta Z$	The Dimensionless Distance Between Two Nodal Points in the Axial Direction	

## Greek Symbols

Symbol	Definition	Unit
$\mu$	Dynamic Viscosity	N.s/m <sup>2</sup>
$\rho$	Density of Fluid	kg/m <sup>3</sup>
$\delta$	Hydrodynamic Boundary Layer Thickness in entrance region	m
$\delta_a$	Hydrodynamic Boundary Layer Thickness in annulus region	m
$\delta_i$	Hydrodynamic Boundary Layer Thickness in internal region	m

## Subscripts

Symbol	Definition	Unit
j,k	The Index Increment Along the Axial and Radial Direction	
i	Inner	
o	Outer	

## 1. Introduction

Flow through circular pipes with concentric disturbed pipe has important industrial applications in the fields of thermal and fluid engineering. Particularly its importance is noted in process industries under particular process requirement and in the design of heat – exchanging equipment. The associated flow patterns developed due to the presence of such disturbed pipe can be quite complex with the development of disturbed zones and their interactions with the confined jet. It has great influence on heat transfer effectiveness and pumping power requirement. This clearly shows the importance of study of such flow hydrodynamics. The model geometry is shown in figure (1). Few works have been reported for flow disturbed by concentric circular pipes.

**Mohammad** [8] numerically studied the problem of steady laminar forced convection in the entry region of concentric annuli with rotating inner walls using fluent code. Due to the axis-symmetry of the problem, a 2D axis-symmetric model is used. Focus is on rotation number (Ro), annulus radius ratio (N) effects on heat transfer characteristics, and the torque required to rotate the inner walls. Air and engine oil were used in the simulation. Reynolds number (Re) of 500 based on inlet velocity and hydraulic diameter is kept constant over the whole range of the considered rotation numbers and radius ratios.

**Mandal and Chakrabarti** [7] numerically investigated disturbances of blood flow through a stenotic coronary artery for the restrictions of 10% to 90% with the Reynolds numbers ranging from 25 to 375. Atherosclerotic plaque formation tends to start from very low flow Reynolds number of 25 with 50% restriction. For Reynolds numbers of 100 and above, it starts at 30% stenosed condition. Impact of percent stenosis on wall shear stress has been noted to be more effective than Reynolds number.

**Founargiotakis et al.** [3] presented an integrated approach for the flow of Herschel–Bulkley fluids in a concentric annulus, modeled as a slot, covering the full range of flow types, laminar, transitional, and turbulent. Prior analytical solutions for laminar flow are utilized. Turbulent flow solutions are developed using the Metzner–Reed Reynolds number after determining the local power law parameters as functions of flow geometry and the Herschel–Bulkley rheological parameters. The friction factor is estimated by modifying the pipe flow equation. Transitional flow is solved introducing transitional Reynolds numbers which are functions of the local power law index.

**Nam and Young** [9] numerically investigated the rotating flow in an annulus. The mean diameter of particles was 0.1 cm and a material density of 2.55 g/cm<sup>3</sup> were used in the experiment.

**Hua-Shu** et al. [4] studied integrated axial flow in an annulus between two concentric cylinders. The critical condition for turbulent transition in annulus flow is calculated with the energy gradient method for various radius ratios. The critical flow rate and critical Reynolds number are given for various radius ratios. The critical condition for the instability of full-developed laminar flow in an annulus is given following the “energy gradient method.” The criterion for instability is based on the energy gradient method for parallel flow instability. It is shown that the critical flow rate and the critical Reynolds number for onset of turbulent transition increase with the radius ratio of the annulus.

The purpose of the current work is to solve the two-dimensional developing laminar flow in the entrance and disturbed regions of concentric circular pipes for a wide range of Reynolds number from 25 to 375.

## 2. Theoretical Formulation

The mathematical analysis is presented for the Partial Differential Equations which describe developing laminar fluid flow in concentric circular pipes. Steady, Incompressible, Newtonian and constant property flow is assumed for developing velocity profile in the entrance region and disturbed region of the concentric circular pipes. One other aspect of this type model is that the velocity profile at the inlet to the main pipe is assumed to be uniform. The details of the geometry under study are shown in figure(1). The flow field is determined by solving the following equations in the computational domain using an implicit finite difference scheme.

### 2.1. Governing Equations

#### 2.1.1. Equation of Continuity:

$$r \frac{\partial u}{\partial z} + \frac{\partial (vr)}{\partial r} = 0 \quad (1)$$

#### 2.1.2. Equation of Momentum:

$$u \frac{\partial u}{\partial z} + v \frac{\partial u}{\partial r} = - \frac{1}{\rho} \frac{dp}{dz} + \nu \left( \frac{\partial^2 u}{\partial r^2} + \frac{1}{r} \frac{\partial u}{\partial r} \right) \quad (2)$$

## 2.2. Boundary Conditions

The requirement that the dependent variable or its derivative must be satisfied on the boundary of the partial differential equation is called the boundary condition. the boundary conditions according to the geometry will be written as follows

### 2.2.1. Entrance Region Boundary Conditions

Uniform velocity profile at the entrance region of main circular pipe is assumed. All entrance boundary conditions can be written as follows [Hornbeck, 1973]:

$$\left. \begin{aligned} u(0, r) &= u_o \\ v(0, r) &= 0 \\ p(0) &= p_o \end{aligned} \right\} \quad (3)$$

#### 2.2.1.1. Wall Boundary Conditions:

All velocity components are zero at walls, hence:

$$\left. \begin{aligned} u(z, r_o) &= 0 \\ v(z, r_o) &= 0 \end{aligned} \right\} \quad (4)$$

#### 2.2.1.2. Centerline of circular pipe Boundary Conditions (symmetry line):

$$\left. \begin{aligned} \frac{\partial u}{\partial r}(z, 0) &= 0 \\ v(z, 0) &= 0 \end{aligned} \right\} \quad (5)$$

## 2.2.2. DISTurbed Region Boundary Conditions

### 2.2.2.1. Wall Boundary Conditions:

$$\left. \begin{aligned} u(z, r_i) &= 0 \\ u(z, r_o) &= 0 \\ v(z, r_i) &= 0 \\ v(z, r_o) &= 0 \end{aligned} \right\} \quad (6)$$

### 2.2.2.2 Centerline of circular pipe Boundary Conditions (symmetry line):

$$\left. \begin{aligned} \frac{\partial u}{\partial r}(z, 0) &= 0 \\ v(z, 0) &= 0 \end{aligned} \right\} \quad (7)$$

### 2.3. The Dimensionless Quantities

Before undertaking a numerical solution, the first step should invariably place the equations to be solved in a dimensionless form having as few parameters as possible. This may be accomplished for equations (1) and (2) by employing the following dimensionless variables :-

$$\left. \begin{aligned} U &= \frac{u}{u_o} \\ V &= \frac{v}{u_o} \\ Z &= \frac{z}{d} \\ R &= \frac{r}{d} \\ P &= \frac{p}{\rho u_o^2} \end{aligned} \right\} \quad (8)$$

Where the characteristic velocity  $u_o$  will usually be chosen as the upstream velocity from the body, and a typical length  $d$  is diameter of main circular pipe.

The following dimensionless quantity will be used in the present work:

$$Re = \frac{\rho \cdot u_o \cdot d}{\mu} \quad (\text{Reynolds number}) \quad (9)$$

### 2.4. Dimensionless Governing Equations

The continuity equation may be made dimensionless by the choice of the dimensionless variables shown in equation (8):

#### 2.4.1. Continuity equation:

$$R \frac{\partial U}{\partial Z} + \frac{\partial (VR)}{\partial R} = 0 \quad (10)$$

The momentum equation may be made dimensionless by the choice of the dimensionless variables of (8) and (9):

#### 2.4.2. Momentum equation:

$$U \frac{\partial U}{\partial Z} + V \frac{\partial U}{\partial R} = - \frac{dP}{dZ} + \frac{1}{Re} \left( \frac{\partial^2 U}{\partial R^2} + \frac{1}{R} \frac{\partial U}{\partial R} \right) \quad (11)$$

### 2.5. Dimensionless Boundary Conditions

The boundary conditions may be made dimensionless by the choice of the dimensionless variables (8) :

### 2.5.1. Entrance Region Dimensionless Boundary Conditions

All entrance dimensionless boundary conditions can be written as follows :

$$\left. \begin{aligned} U(0, R) &= 1 \\ V(0, R) &= 0 \\ P(0) &= 1 \end{aligned} \right\} \quad (12)$$

#### 2.5.1.1 Wall Dimensionless Boundary Conditions:

All dimensionless velocity components are zero at walls, hence:

$$\left. \begin{aligned} U(Z, 1) &= 0 \\ V(Z, 1) &= 0 \end{aligned} \right\} \quad (13)$$

#### 2.5.1.2. Centerline of circular pipe dimensionless Boundary Conditions:

At centerline of the duct the dimensionless boundary conditions are:

$$\left. \begin{aligned} \frac{\partial U}{\partial R}(Z, 0) &= 0 \\ V(Z, 0) &= 0 \end{aligned} \right\} \quad (14)$$

### 2.5.2. Disturbed Region Dimensionless Boundary Conditions

#### 2.5.2.1 Wall Dimensionless Boundary Conditions:

All dimensionless velocity components are zero at walls, hence:

$$\left. \begin{aligned} U(Z, 0.5) &= 0 \\ V(Z, 0.5) &= 0 \end{aligned} \right\} \quad (15)$$

#### 2.5.2.2 Centerline of circular pipe dimensionless Boundary Conditions:

$$\left. \begin{aligned} \frac{\partial U}{\partial R}(Z, 0) &= 0 \\ V(Z, 0) &= 0 \end{aligned} \right\} \quad (16)$$

## 2.6. Numerical Formulation for Momentum and Continuity Equations

The Finite Difference Method (FDM) will be used to solve the momentum equation for a steady, two-dimensional, laminar, constant-property boundary-layer flow of a Newtonian fluid. The difference grid is shown in figure (2). Equations (10) and (11) are expressed in difference form as:

$$\frac{R_k (U_{j+1,k} - U_{j,k})}{2(\Delta Z)} + \frac{R_{k+1} (U_{j+1,k+1} - U_{j,k+1})}{2(\Delta Z)} + \frac{V_{j+1,k+1} R_{k+1} - V_{j+1,k} R_k}{\Delta R} = 0 \quad (17)$$



$$U_{j,k} \frac{U_{j+1,k} - U_{j,k}}{\Delta Z} + V_{j,k} \frac{U_{j+1,k+1} - U_{j+1,k-1}}{2(\Delta R)} = -\frac{P_{j+1} - P_j}{\Delta Z} + \frac{1}{\text{Re}} \left( \frac{U_{j+1,k+1} - 2U_{j+1,k} + U_{j+1,k-1}}{(\Delta R)^2} + \frac{1}{R_k} \frac{U_{j+1,k+1} - U_{j+1,k-1}}{2(\Delta R)} \right) \quad (18)$$

Equations (17) and (18) written for  $k=1(1)n$ .

## 2.7. Validation

As a first validation case, the flow in circular pipe disturbed by concentric circular pipe is solved. The geometry and the boundary conditions are indicated in Figure (1). Flow through this configuration is analyzed at different Reynolds number. Tables (1) present the validation of pressure gradient. Table (2) present the validation of velocity profile for flow through concentric circular pipes. The validity of results is verified and shows that there is a good agreement between the results of the present solution and the AutoFEA software.

## 3. Results and Discussion

The results obtained from the numerical solution by using the computer program which was prepared for this purpose. for Reynolds numbers (Re=25), (Re=50), (Re=100), (Re=200) and (Re=375). The nodal spacing is constant across the axial direction and radial direction.  $(m*(2*(n+1)+1))$  represents the number of nodal points for concentric circular pipes. The concentric circular pipes problem was solved with  $(n=5)$ , but  $(m)$  varied corresponding on Reynolds number (i.e., when the Reynolds number is 25,  $m=30$ ).

### 3.1. Velocity Variation

Figures (3), (4), (5), (6) and (7) show the velocity profiles which manifest stages of developing the hydrodynamic boundary layer for Reynolds numbers (Re=25), (Re=50), (Re=100), (Re=200) and (Re=375) at different sections of the concentric circular pipes. The velocity in the inlet section of main pipe is uniform and its magnitude is  $(U=U_0=1)$ . The velocity profile in the inlet section of disturbed circular pipe is uniformly distributed over its diameter and the velocity distribution becomes parabolic. The radial velocity component (V) is zero. The axial velocity increasing until it approaches maximum in centerline of disturbed pipe. The velocity profile in the annulus concentric section of disturbed pipe is non-uniformly distributed. The velocity near the main pipe is less than the velocity near the disturbed pipe, due to the effect of velocity at inlet annulus section. The shape of the boundary layer becomes constant after a certain distance from the entrance, which is so-called "The Hydrodynamic Entry length". It is noted that the hydrodynamic entrance length increases with the increasing of Reynolds number. It can be seen that the boundary layer is developed faster for the lower Reynolds number, however the flow field is similar for all studied cases. At a large distance from the inlet the velocity distribution becomes parabolic. The resulting velocity profile

consist of two boundary layer profiles on the two walls joined in the center by a line of constant velocity. Since the volume flow rate is constant, the decrease in the flow rate near the walls which is due to friction must be compensated by a corresponding increase near the axis. Figures (8), (9), (10), (11) and (12) show the axial dimensionless velocity development as a function of  $Z$  for different radial positions and Reynolds numbers. The dimensionless velocity at inlet equal one. In the developing region the dimensionless velocity increases near the centerline of pipe with increases dimensionless axial position but decreases the dimensionless velocity near the wall of pipe with increases dimensionless axial position. In the disturbed region the dimensionless velocity increases at near the wall and centerline of pipe but decreases at  $R=0.33333$  due to the axial flow rate constant at any section.

Figure (13) shows the velocity profiles in the entrance region at different Reynolds numbers. In the developing region the maximum velocity decreases with increasing Reynolds number but the velocity near the wall increases with increasing Reynolds number. In the fully developed region all values of Reynolds number have the same velocity profile (the velocity profiles in fully developed is independent of Reynolds number).

Figure (14) shows the velocity profiles in the disturbed region at different Reynolds numbers. The velocity at the wall equals zero but the axial velocity near the core increases. The maximum velocity decreases with increasing Reynolds number but the velocity near the wall increases with increasing Reynolds number. At a large distance from the inlet of disturbed pipe the velocity distribution becomes parabolic. At inlet of annulus region the velocity near the main circular pipe is less than velocity near the disturbed circular pipe until they equal at a certain distance from the entrance.

### **3.2. Pressure Variation**

Figure (15) shows dimensionless pressure variation in entrance region at different Reynolds numbers. The dimensionless pressure in the inlet section is one and decreases with increasing distance in  $Z$ -direction due to friction. The dimensionless pressure decreases faster with the decreases of Reynolds number.

Figure (16) shows dimensionless pressure variation in internal and annulus region at different Reynolds numbers. The dimensionless pressure decreases with increasing distance in  $Z$ -direction. The pressure drop in annulus region is greater than pressure drop in the inside region.

## **4. Conclusions**

The axial velocity increasing until it approaches maximum in centerline of disturbed pipe. The velocity profile in the annulus concentric section of disturbed pipe is non-uniformly distributed.

The velocity near the main pipe less than the velocity near the disturbed pipe due to the effect of velocity at inlet annulus section. Since the volume flow rate is constant, the decrease in the flow rate near the walls which is due to friction must be compensated by a corresponding increase near the axis. In the entrance region the maximum velocity decreases with increasing Reynolds number but the velocity near the wall increases with increasing Reynolds number. The velocity profiles in fully developed is independent of Reynolds number. At a large distance from the inlet of disturbed pipe the velocity distribution becomes parabolic. The dimensionless pressure in the inlet section is one and decreases with increasing distance in Z-direction due to friction. The dimensionless pressure decreases faster with the decreases of Reynolds number. The pressure drop in annulus region is greater than pressure drop in the inside region.

## **5. References**

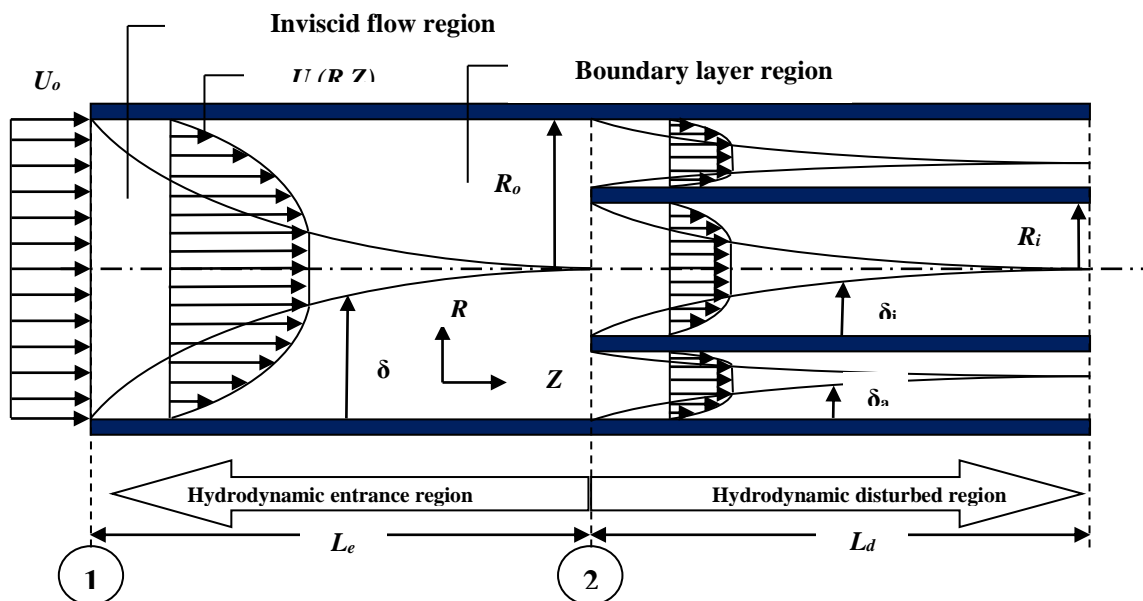
- [1] Adams, J.A. and Rogers D.F. **“Computer-Aided Heat Transfer Analysis”**, McGraw-Hill Book Company, New York., 1973
- [2] Anderson, D.A., Tannehill, J.C., and Pletcher, R.H. **“Computational Fluid Mechanics and Heat Transfer”**, McGraw-Hill Book Company, New York., 1984
- [3] Founargiotakis K., Kelessidis V.C. and Maglione R. **“Laminar, transitional and turbulent flow of Herschel-Bulkley fluids in concentric annulus”** , the Canadian Journal of Chemical Engineering, Vol. 86, pp. 676-683, August 2008.
- [4] Hua-Shu Dou, Boo Cheong Khoo and Her Mann Tsai **“Determining the critical condition for low transition in a full-developed annulus flow”** , Journal of Petroleum Science and Engineering, Vol. 71, 2010, in press.
- [5] Hornbeck, R.W. **“Numerical Marching Techniques for Fluid Flows with Heat Transfer”**, National Aeronautics and Space Administration, Washington., 1973
- [6] Incropera, F.P. and Dewitt, D.P. **“Fundamentals of Heat and Mass Transfer”**, John Wiley & Sons, New York., 1996
- [7] Mandal D.K. and Chakrabarti S. **“Two dimensional simulation of steady blood flow through a stenosed coronary artery”** , International Journal of Dynamics of Fluids, ISSN 0973-1784, Vol. 3, No. 2, pp. 187-209, 2007.
- [8] Mohammad Abdulrahman Al-Shibl **“Prediction of Flow and Heat Transfer in the Entry Region of Concentric Cylinders with Rotating Inner Walls”** , M.Sc. thesis, Mechanical Engineering Department, King Fahd University of Petroleum and Minerals, 2006.
- [9] Nam Sub Woo and Young Kyu Hwang **“A Study on the Rotating Flow in an Annulus”**, International Offshore and Polar Engineering Conference Vancouver, BC, Canada, July 6-11, 2008.

**Table (1): Validation Data for Flow through concentric circular pipes.**

Entrance Length [Le]		Pressure Gradient [dP/dZ] at Disturbed Region		Pressure Gradient [dP/dZ] at Entrance Region		Re
AutoFEA	present work	AutoFEA	present work	AutoFEA	present work	
2.5	2.5	0.26	0.2687064	0.538	0.5481035	25
5	5	0.257	0.2655766	0.529	0.5390269	50
10	10	0.243	0.2517739	0.525	0.5350066	100
20	20	0.237	0.245094	0.523	0.5331393	200
37.5	37.5	0.232	0.2403765	0.522	0.5323037	375

**Table 3: Developing Velocity Profile for Flow through concentric circular pipes**

Re=375		Re=200		Re=100		Re=50		Re=25		R
U(Z=1)		U(Z=1)		U(Z=1)		U(Z=1)		U(Z=1)		
AutoFEA	present work	AutoFEA	present work	AutoFEA	present work	AutoFEA	present work	AutoFEA	present work	
1.02	1.020837	1.04	1.038549	1.07	1.074004	1.13	1.133734	1.22	1.217645	0
1.02	1.020837	1.04	1.038538	1.07	1.073871	1.13	1.132324	1.21	1.20985	0.1666667
1.02	1.020823	1.04	1.038397	1.07	1.072529	1.12	1.123713	1.18	1.176898	0.3333334
1.02	1.020451	1.04	1.036447	1.06	1.062581	1.09	1.087019	1.09	1.087502	0.5
1.01	1.013298	1.02	1.015547	1.01	1.004406	0.96	.9613851	0.89	.8887085	0.6666667
0.92	.9141725	0.85	.8517973	0.75	.7496103	0.63	.6286924	0.53	.5282193	0.8333334
0	0	0	0	0	0	0	0	0	0	1

**FIGURE (1): Laminar, hydrodynamic boundary layer development in a concentric circular pipe.**

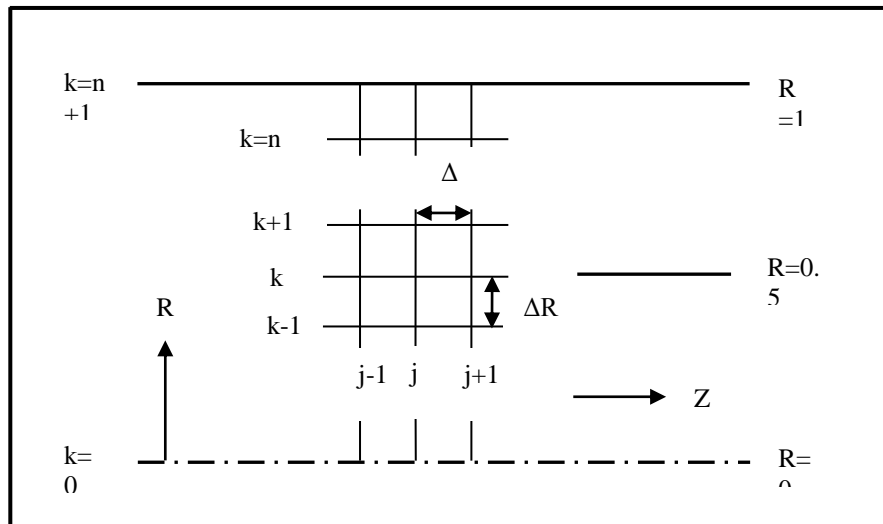


**FIGURE (2): Finite Difference Grid For concentric circular**

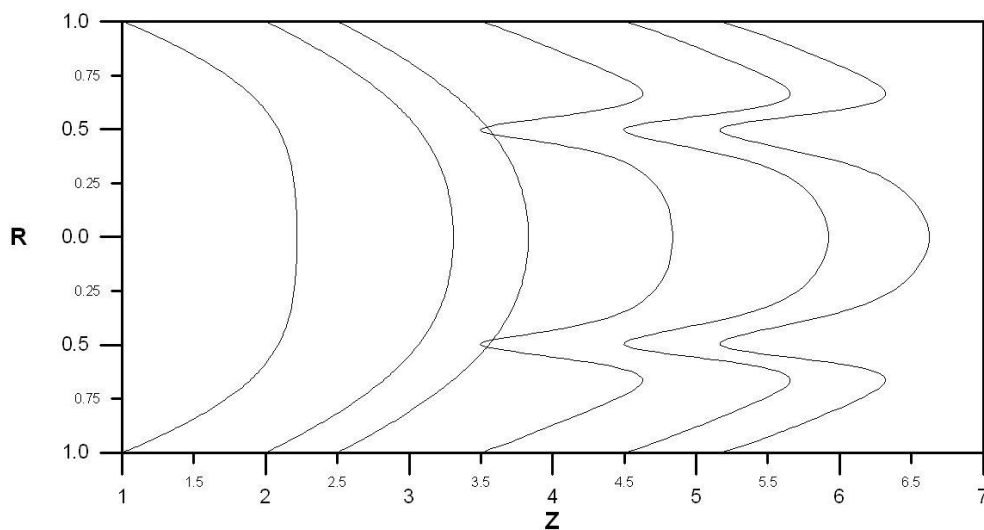


**FIGURE (3): Axial velocity profiles at different axial locations**

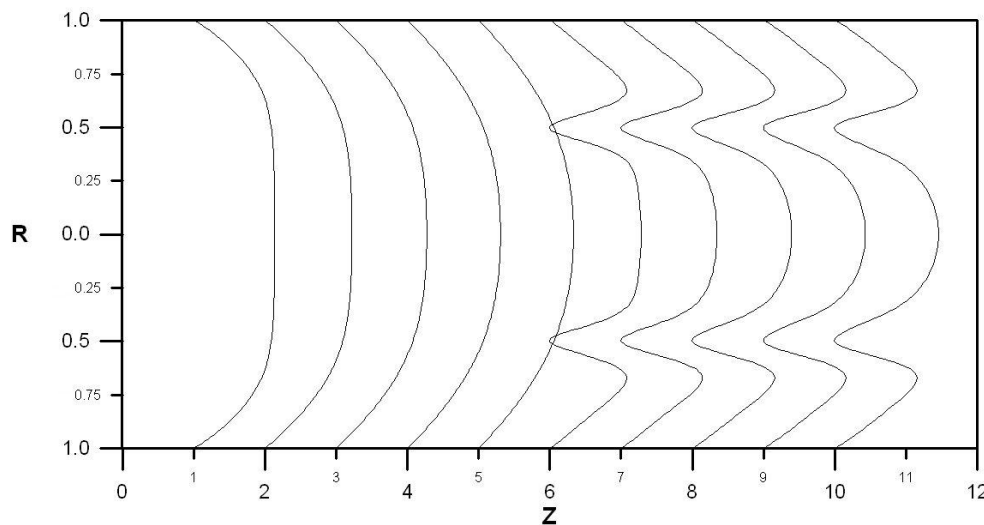


**FIGURE (4): Axial velocity profiles at different axial locations for Re=50**

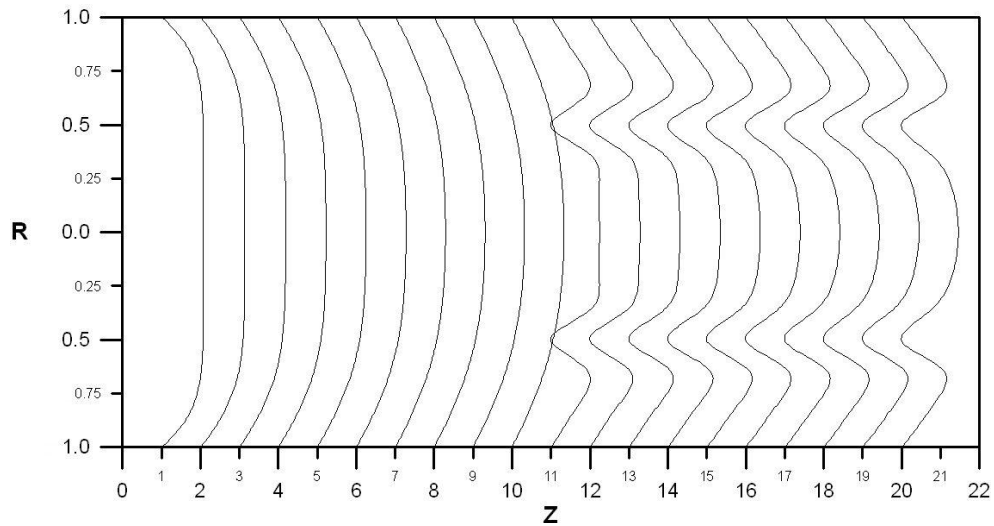


**FIGURE (5): Axial velocity profiles at different axial locations for  $Re=100$**

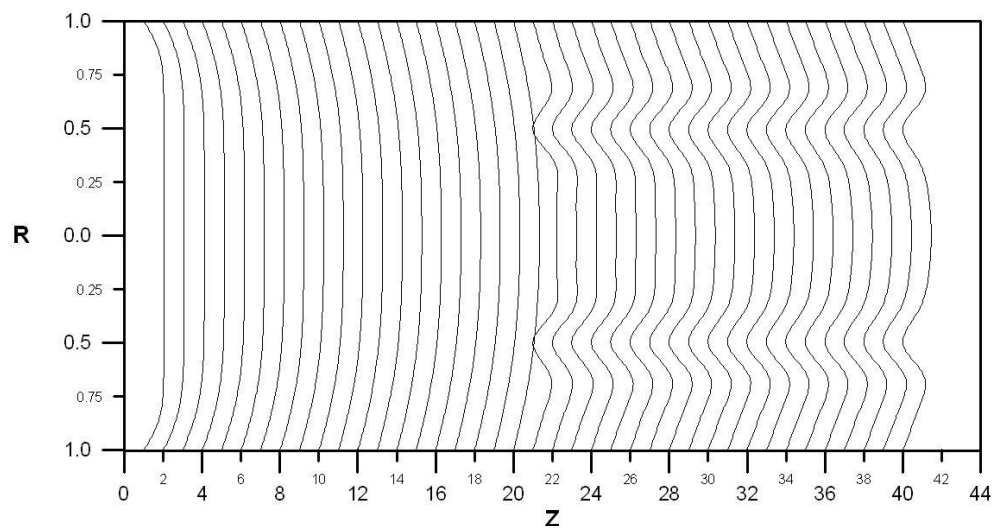


**FIGURE (6): Axial velocity profiles at different axial locations for  $Re=200$**

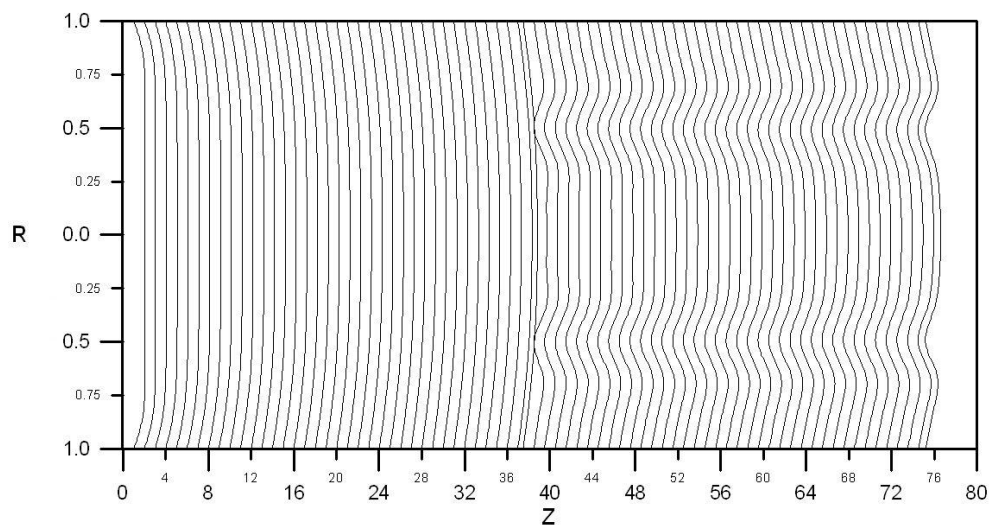


**FIGURE (7): Axial velocity profiles at different axial locations for  $Re=375$**

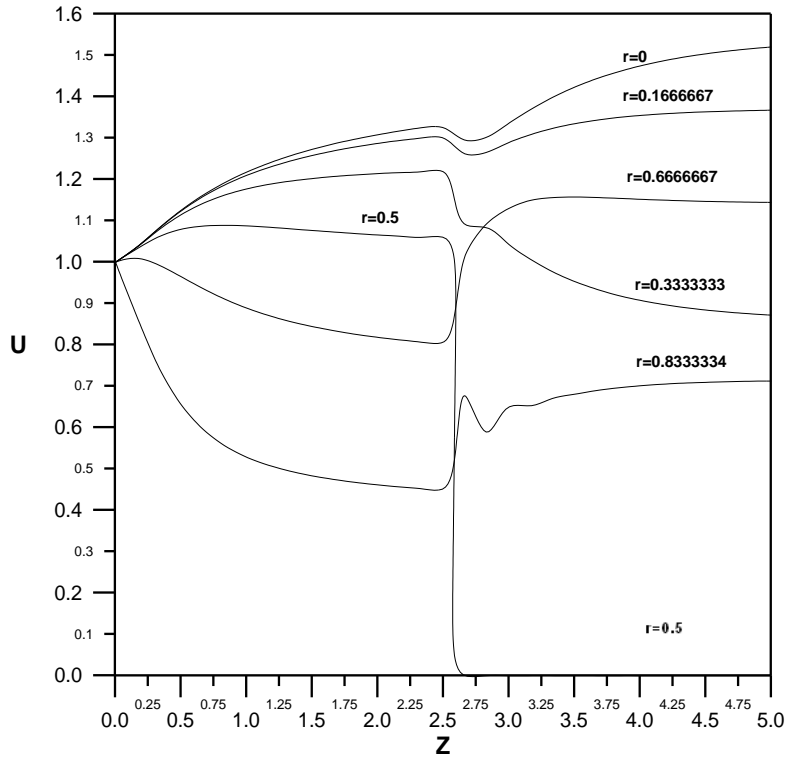


**FIGURE (8): Dimensionless axial velocity development in concentric circular pipe for various dimensionless radial positions, at  $Re=25$**

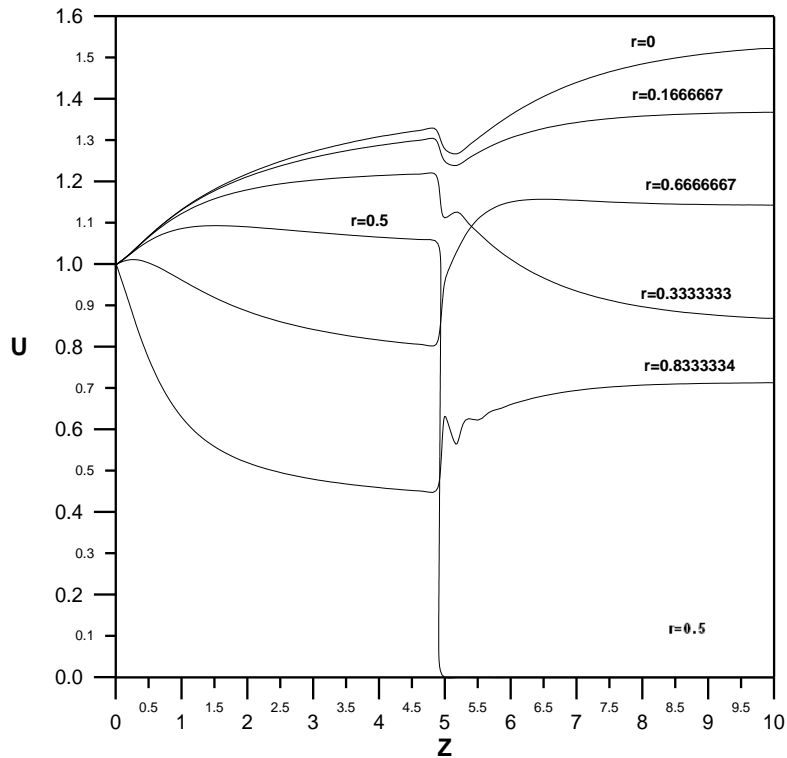


**FIGURE (9): Dimensionless axial velocity development in concentric circular pipe for various dimensionless radial positions, at  $Re=50$**

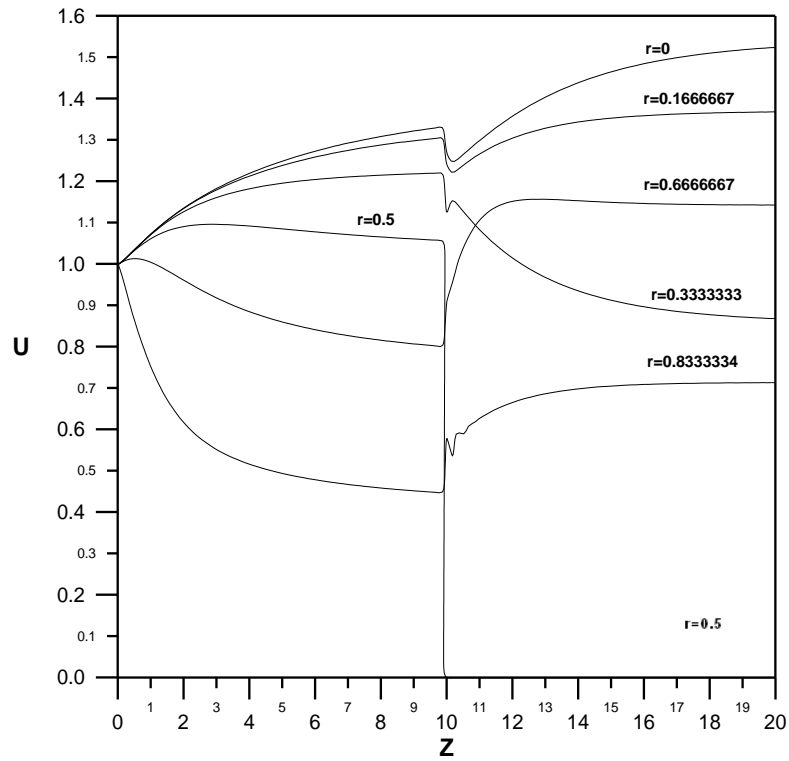


**FIGURE (10): Dimensionless axial velocity development in concentric circular pipe for various dimensionless radial positions, at  $Re=100$**

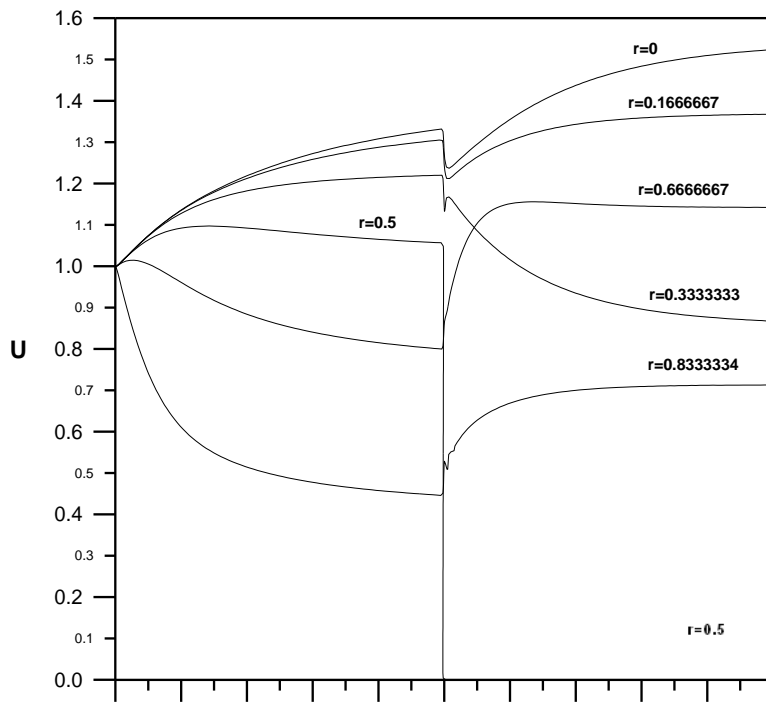


**FIGURE (11): Dimensionless axial velocity development in concentric circular pipe for various dimensionless radial positions, at  $Re=200$**



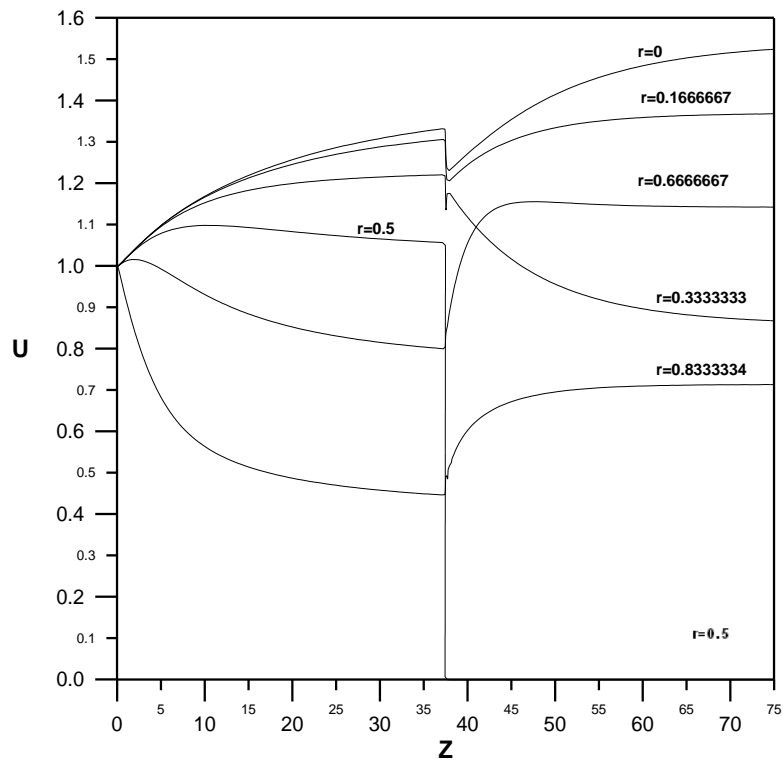


**FIGURE (12): Dimensionless axial velocity development in concentric circular pipe for various dimensionless radial positions, at  $Re=375$**

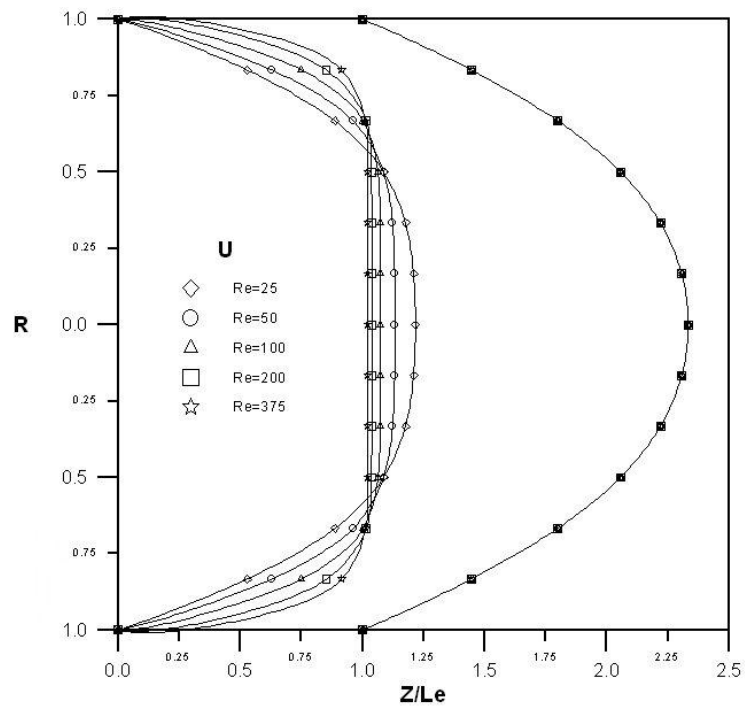


**FIGURE (13): Developing and fully developed velocity profile in entrance region of circular pipe, for different Reynolds number.**

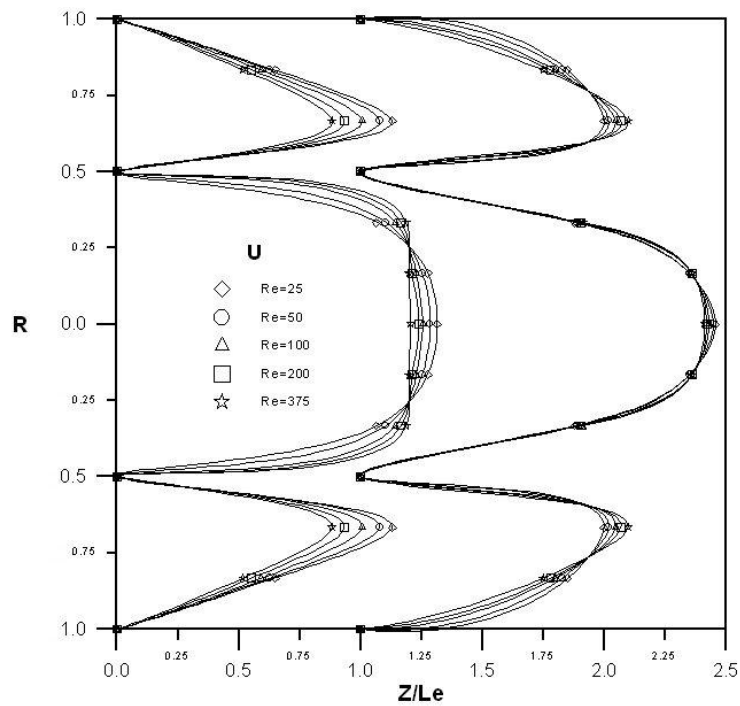


**FIGURE (14):** Developing and fully developed velocity profile in disturbed region of concentric circular pipes, for different Reynolds number.

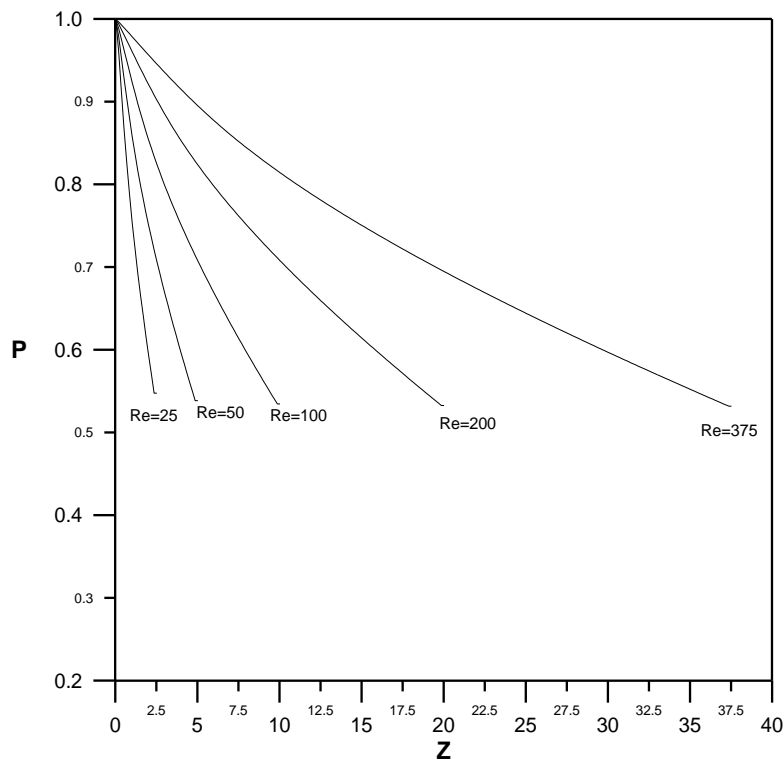


**FIGURE (15):** Pressure variation in entrance region of circular pipe, for different Reynolds number.

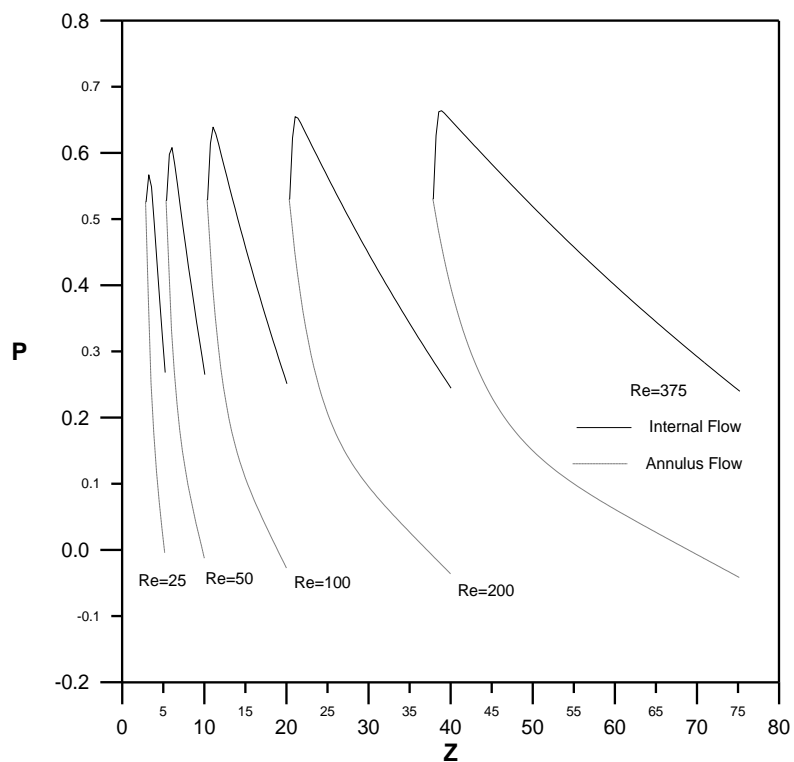


**FIGURE (16): Pressure variation in disturbed region of concentric circular pipe, for different Reynolds number.**